Arch. Metall. Mater. **64** (2019), 1, 45-53

DOI: 10.24425/amm.2019.126217

A. GÓRAL*#, W. ŻÓRAWSKI**

EFFECT OF POWDER GRAIN SIZE AND TITANIA CONTENT ON MECHANICAL AND TRIBOLOGICAL PROPERTIES OF PLASMA SPRAYED Al_2O_3-TiO_2 CERAMIC COATINGS

In this work, three ceramic composite coatings Al_2O_3-3TiO_2 C, Al_2O_3-13TiO_2 C, and Al_2O_3-13TiO_2 N were plasma sprayed on steel substrates. They were deposited with two conventional powders differing the volume fraction of TiO_2 and nanostructured powder. The mechanical and tribological properties of the coatings were investigated and compared. The increase in TiO_2 content from 3 wt.% to 13 wt.% in the conventional feedstock improved the mechanical properties and abrasion resistance of coatings. However, the size of the used powder grains had a much stronger influence on the properties of deposited coatings than the content of the titania phase. The Al_2O_3-13TiO_2 coating obtained from nanostructured powder revealed significantly better properties than that plasma sprayed using conventional powder, i.e. 22% higher microhardness, 19% lower friction coefficient, and over twice as good abrasive wear resistance. In turn, the Al_2O_3-13TiO_2 conventional coating showed an increase in microhardness and abrasive wear resistance, 36% and 43%, respectively, and 6% higher coefficient of friction compared to the Al_2O_3-3TiO_2 conventional coating.

Keywords: Al_2O_3-TiO_2 coating, Nanostructures, Mechanical properties, Wear resistance

1. Introduction

There is a growing industrial need for technologies allowing to manufacture coatings that would ensure the protection of machine parts. Among the materials most widely used as wear and corrosion resistant deposits are ceramic coatings. Alumina-titania ceramic coatings possess attractive properties, such as high hardness, low density, high melting point, low thermal expansion and excellent corrosion resistance. This enables them to find applications in microelectronics, automotive and friction materials [1,2]. Additionally, they are characterized by enhanced toughness and wear resistance when compared to monolithic Al_2O_3 coatings [3,4]. The addition of TiO_2 phase effectively toughens the matrix of Al_2O_3 coatings [5-6]. Titania solute in alumina can improve the ductility, shock resistance and bonding strength of the coatings [7-9]. These coatings are usually manufactured using the plasma spraying process, as the high temperature of the plasma flame allows for the melting of the ceramic powder particles. The high velocity oxygen fuel (HVOF) spraying method may also be used, however, in this process, quite often, fewer melt particles are found [10]. Moreover, it is expected that spraying with nanocrystalline powders will allow for producing deposits with improved properties (hardness, bonding strength and crack growth resistance) than using conventional Al_2O_3-TiO_2 powders [11-13]. In recent times, the plasma spraying process has created opportunities to develop high performance nanostructured ceramic coatings with superior mechanical and wear properties, as well as creep resistance [7-8,14-18]. However, due to the nanostructured powders being too small and too light to be carried by the gas stream and deposited on a substrate during this process, the powders should be reconstituted into porous spherical micron-sized agglomerates [5]. The alumina-titania coatings are very popular, due to the possibility of obtaining deposits with enhanced properties. Many studies have been carried out characterizing the influence of the powders' morphology and manufacturing methods [19-20], grain size [21-23], chemical composition [5,24-27], process parameters [6-7,28-30] on the hardness and wear resistance. Despite the existence of numerous articles related to the microstructure and the properties of Al_2O_3-TiO_2 coatings [2,5-9,11,15-17,19-30], it has not been fully explained which parameter, i.e. powder morphology or chemical composition, has a greater impact on the tribological properties of coatings. A novelty of this paper is linking the mechanical properties (microhardness, wear resistance, coating adhesion, coefficient of friction) with the microstructure of nanostructured and conventional plasma sprayed Al_2O_3-TiO_2 coatings.

2. Material and methods

The coatings were plasma sprayed using the Plancer PN-120 system equipped with the Thermal Miller 1264 powder

* INSTITUTE OF METALLURGY AND MATERIALS SCIENCE, POLISH ACADEMY OF SCIENCES, REYMONTA 25, 30-059 KRAKOW, POLAND,
** LASER PROCESSING RESEARCH CENTRE, KIELCE UNIVERSITY OF TECHNOLOGY, 7 TYSIĄCLECIA PAŃSTWA POLSKIEGO AV., 25-314 KIELCE, POLAND
# Corresponding author: a.goral@imim.pl

feeder. The feedstock compositions were a commercially achievable mixture of conventional (C) Al_2O_3 and TiO_2 powders (Al_2O_3:TiO_2 wt.% ratio was 87:13 and 97:3 for Amdry 6228 and FST C-328.25, respectively) and nanostructured (N) Al_2O_3-$13TiO_2$ powder (Infralloy Nanox S2613S). The conventional coatings were denoted as Al_2O_3-$3TiO_2$ C and Al_2O_3-$13TiO_2$ C, respectively, and the nanostructured Al_2O_3-$13TiO_2$ N. The coatings were deposited on low-carbon steel substrates. Before spraying, the substrates were degreased and grit blasted with electrocorundum EB-12 (1700÷2000 μm) at the pressure of 0.5 MPa. The plasma spraying parameters of the coatings are presented in Table 1. The thickness of the coatings was in the range of 0.35÷0.5 mm.

TABLE 1

Parameters of Al_2O_3-TiO_2 plasma sprayed coatings

Current [A]	Voltage [V]	Plasma gas pressure [MPa]	Spraying distance [mm]	Powder feeding rate [g/min]	Spraying velocity [m/s]
550	55	0.7	100	90	0.3

Measurement of microhardness was made under the load of 100 mN and their corresponding rise and fall rates of 200 mN/s according to PN-EN ISO 14577-1. The maintenance time at maximum load was 5 s. For each sample, 7 measurements on their cross section were taken at each load. A small load was applied to measure microhardness values to ensure the proper correlation of results with the real properties of the coating not including microstructure defects like pores and voids.

Calculation of Young's modulus (E_{IT}) and hardness (H_{IT}) was done according to standard Olivier & Pharr method (MCT) [31] $E_r = \frac{\sqrt{\pi}\cdot S}{2\cdot\sqrt{A}}$ where S is the stiffness, A is the contact area of the indentation, at the maximum load. The specimen's Young's modulus, E, is obtained using the definition $\frac{1}{E_r} = \frac{1-\nu^2}{E} + \frac{1-\nu_i^2}{E_i}$ where E and ν are the Young's modulus and the Poisson's ratio of the specimen and of the indenter (i).

Tribological tests were performed using a CSM Instruments tribometer applying the ball on disc method. The tests were performed according to ASTM G 99-05, ISO 20808: 2004. These tests were carried out on the polished coatings surfaces (Ra < 0.1 μm). A counter-part was 6 mm diameter ball made of 100Cr6 steel. Process parameters were as load 5 N, speed 0.1 ms^{-1}, distance 2000 m, radius of the wear trace 0.019 m. The tangential force F_t was recorded, and the coefficient of friction for this pair was calculated according to the dependence $f = F_t/F_n$ where f – coefficient of friction, F_t – tangential force, F_n – normal force.

The scratch test was performed on an MCT using a Rockwell C diamond indenter with a radius of 200 μm. Length of the scratch was 5 mm. The maximum load P_{max} was 30 N. Changes in load values were linear and the range over the entire scratch length was from 0.01 N to 30 N. The penetration rate of the indenter was set to $5\cdot10^{-3}$ m min^{-1}. The tests were carried out in accordance with PN-EN 1071-3. The coating microstructures of wear tracks after scratch test were observed using optical microscope (Leica DM IRM). The abrasive wear resistance tests of deposits were performed using a dry sand rubber wheel tester. The Al_2O_3 powder with a grain size of 300 μm was applied as an abrasive in this test. The worn surfaces were analysed using scanning electron microscope (SEM FEI Novaä NanoSEM 200).

3. Results

3.1. Characterisation of the powder and coating microstructure

The Al_2O_3-$3TiO_2$ C and Al_2O_3-$13TiO_2$ C conventional coatings were deposited using conventional fused and crushed powders, while the Al_2O_3-$13TiO_2$ N was obtained using nanostructured agglomerated powders (10-50 μm). The Al_2O_3-$13TiO_2$ N powder besides α-Al_2O_3 (corundum) and TiO_2 (rutile), contained nanoparticles of ZrO_2 (8 wt.%) and CeO_2 (5 wt.%) additives according to producer specification. The presence of these oxides was confirmed by X-ray diffraction phase analysis of the powder and shown in our earlier paper [32]. ZrO_2 and CeO_2 oxides introduced into the powder reduce a sintering temperature and accelerate the densification of ceramic composite powder [33-34]. The analysis of the grain size distribution of three used powders (Fig. 1 and Table 2) revealed that Al_2O_3-$13TiO_2$ C powder possessed the highest grain size (d_{50} = 38.13 ± 0.14 μm) about twice as large as that of the Al_2O_3-$3TiO_2$ C (d_{50} = 17.68 ± 0.02 μm) powder and up to 35 times greater grain size (d_{50} = 3.59 ± 0.03 μm) than the nanostructured Al_2O_3-$13TiO_2$ N powder determined for fraction d_{50}. The overall particle size distribution of the Al_2O_3-$13TiO_2$ C, from 21.19 to 59.94 μm, was broad when compared to that of the Al_2O_3-$3TiO_2$ C, from 9.17 to 29.84 μm and that of Al_2O_3-$13TiO_2$ N, from 0.59 to 11.56 μm, Fig. 1. Differences in the powder size and form resulted in a dissimilarity of the microstructure of plasma sprayed coatings. The conventional coatings presented typical splat microstructure, Fig. 2. The surface morphology showed the splashes of titania (white phase) into melted alumina phase (dark gray phase); there were some microcracks on the surfaces, Fig. 2a and b. The coatings were composed of elongated TiO_2 bands distributed between Al_2O_3 phase (mainly γ-Al_2O_3 phase, although the α-Al_2O_3 were also observed), Fig. 2d and e [11-13, 32,35]. The micro-pores (larger

TABLE 2

The grain size of the Al_2O_3-TiO_2 powders

	Al_2O_3-$3TiO_2$ C	Al_2O_3-$13TiO_2$ C	Al_2O_3-$13TiO_2$ N
d_{10} [μm]	9.17 ± 0.01	21.19 ± 0.04	0.59 ± 0.02
d_{50} [μm]	17.68 ± 0.02	38.13 ± 0.14	3.59 ± 0.03
d_{90} [μm]	29.84 ± 0.05	59.94 ± 0.20	11.56 ± 0.02

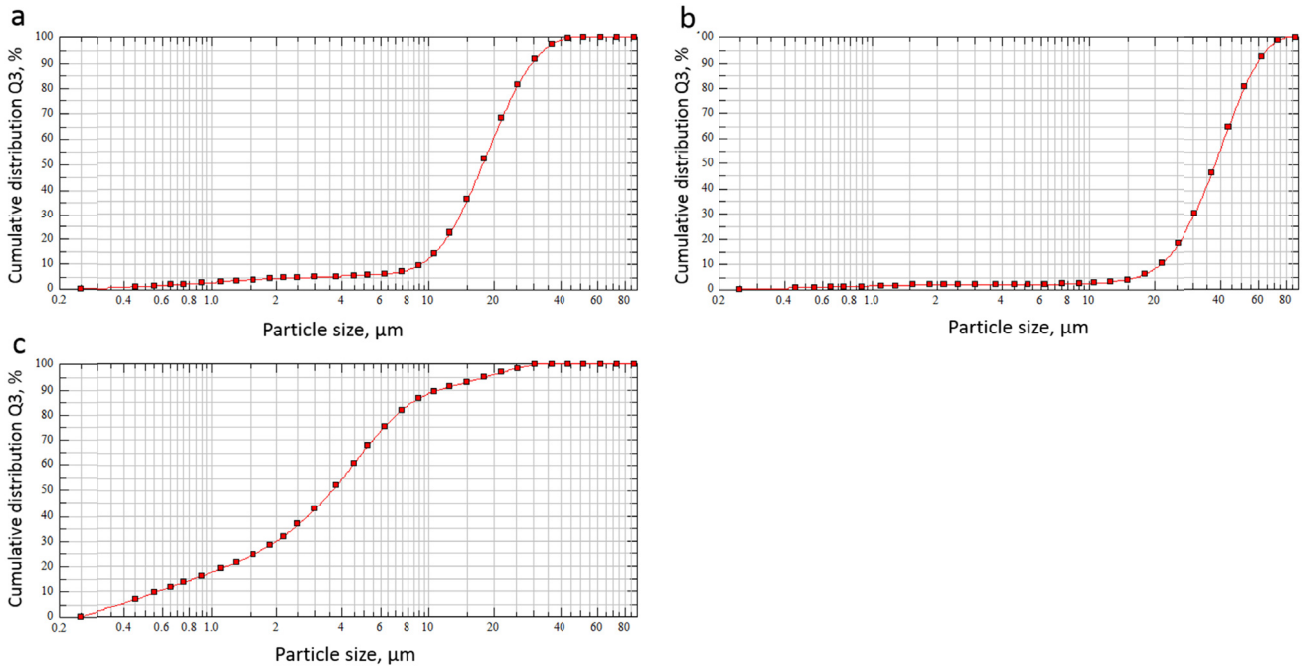

Fig. 1. Grain size distribution analysis of the powders: a) Al_2O_3-3TiO_2 C, b) Al_2O_3-13TiO_2 C, c) Al_2O_3-13TiO_2 N

in the case of Al_2O_3-13TiO_2 C) were defects in these structures, no micro-cracks were observed. The Al_2O_3-13TiO_2 N nanostructured coating consisted of a bi-modal microstructure formed from area constituted from fully melted (FM) oxide particles and region of partially-melted (PM) particles containing some microstructural features of the original particles, Fig. 2c and f. Micro-pores were observed in the microstructure. Similarly, as in the conventional coatings, the splats mainly consisted of nanometer-sized γ-Al_2O_3 growing into various shapes and sizes, the amorphous phase and α-Al_2O_3 phase [12,35]. The partially melted rounded feature consisted of α-Al_2O_3 grains. They were a retained part of the used powder surrounded by a three-dimensional net-like structure formed from fully melted oxides [11-13,32,35].

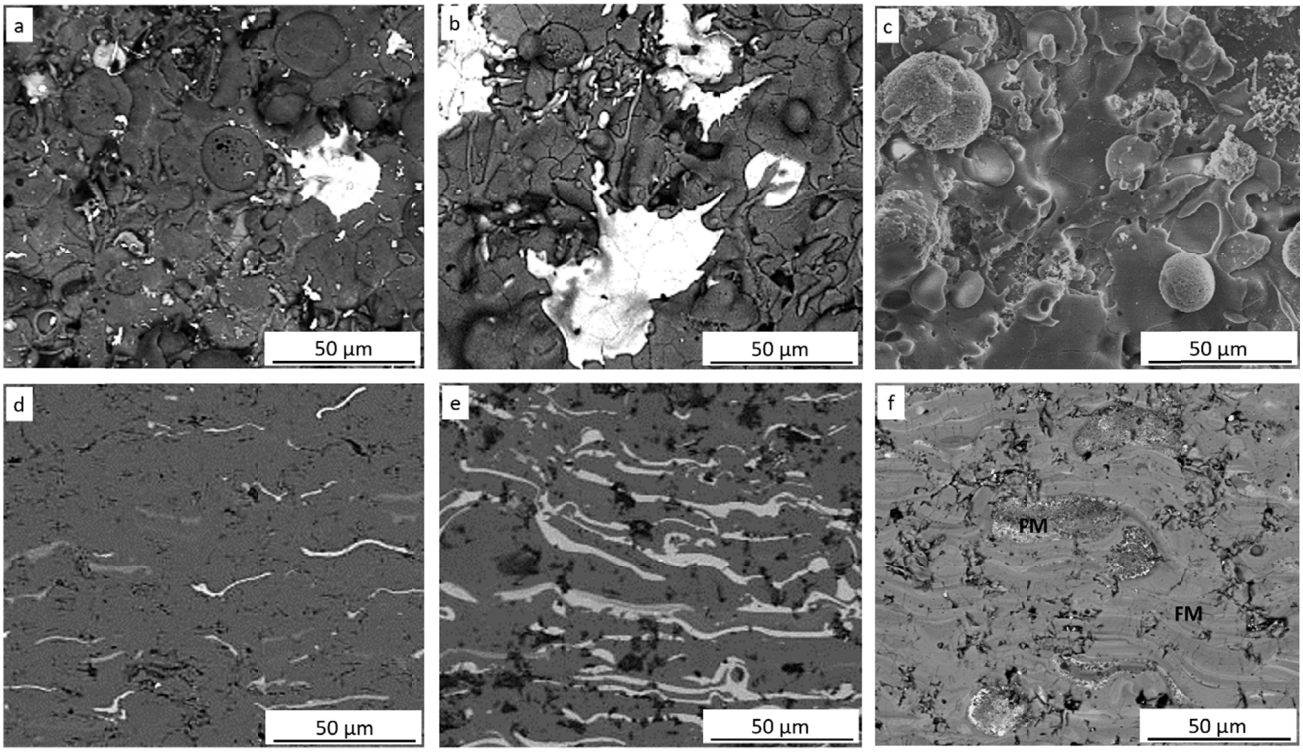

Fig. 2. SEM BSE (backscattered electrons) surface morphologies and cross sections of the coatings a, d) Al_2O_3-3TiO_2 C; b, e) Al_2O_3-13TiO_2 C; c, f) Al_2O_3-13TiO_2 N

3.2. Mechanical and tribological properties of Al_2O_3-3TiO_2 C, Al_2O_3-13TiO_2 C, and Al_2O_3-13TiO_2 N coatings

3.2.1. Mechanical properties

Mechanical properties of the coatings were investigated in terms of microhardness, Young's modulus as listed in Table 3. The microhardness and Young's modulus measurement were performed on the polished cross-sections of the coatings.

It can be seen from Table 3 that the coatings sprayed with nanostructured Al_2O_3-13TiO_2 N feedstock revealed the highest microhardness. This value was significantly higher at 21% and 75% than that of the coatings sprayed with conventional powders Al_2O_3-13TiO_2 C and Al_2O_3-3TiO_2 C, respectively. The similar tendency was shown in the case of Young's modulus of the coatings. The microhardness differences were derived from various microstructure, phase composition and chemical elements distribution in the coatings [35]. The increase in microhardness and Young's modulus in the case of nanostructured coatings could be attributed to a combined effect of bi-modal microstructure composed of partially and fully melted agglomerates of nanoparticles and a decrease in their porosity [11-13,32,35].

TABLE 3

Microhardness (H_{IT}) and Young's modulus (E_{IT}) of the coatings determined under the load of 100 mN

Coating	H_{iT} [GPa]	E_{IT} [GPa]
Al_2O_3-3TiO_2 C	7.2 ± 1.0	102 ± 15
Al_2O_3-13TiO_2 C	10.3 ± 2.0	124 ± 14
Al_2O_3-13TiO_2 N	12.6 ± 1.9	164 ± 19

3.2.2. Tribological properties

Investigations of tribological properties were carried out on the samples with a polished surface. The average roughness (Sa) after polishing was 0.093 μm, 0.095 μm and 0.053 μm for Al_2O_3-3TiO_2 C, Al_2O_3-13TiO_2 C, and Al_2O_3-13TiO_2 N coatings, respectively. The morphologies of the coating surfaces were shown in Fig. 3.

Scratch tests

During scratch tests, no adhesion decline or removal from the substrate was observed for any of the coatings. The high thickness of the coatings prevented the shear stresses in the plane of the coating-steel substrate interface. Microstructure of coating wear tracks after scratch test are shown in Fig. 4. Only cohesive cracks resulting from over-strength of the coating were observed because of high tensile stresses behind the indenter. The load at which such cracks occurred was determined as the first critical load (L_{c1}). Since no adhesion fracture was observed up to the maximum force of 30 N, it was not possible to determine the second critical load (L_{c2}) parameter. The conventional coatings Al_2O_3-3TiO_2 C and Al_2O_3-13TiO_2 C revealed similar properties, Table 4. The first cracks in these coatings formed with the L_{c1} load of 12 N and 16 N, respectively. An increase in the load to 23 N resulted in a significant peeling of the coating. The Al_2O_3-13TiO_2 N coating was more durable compared to the conventional coatings. Although the critical load (22 N) was similar to those of the other coatings, the extent of cracking and crushing of the coating was considerably smaller. The friction coefficient for nanostructured coating determined during the scratch test was significantly lower (0.16) than for the conventional coatings (0.21), Table 4.

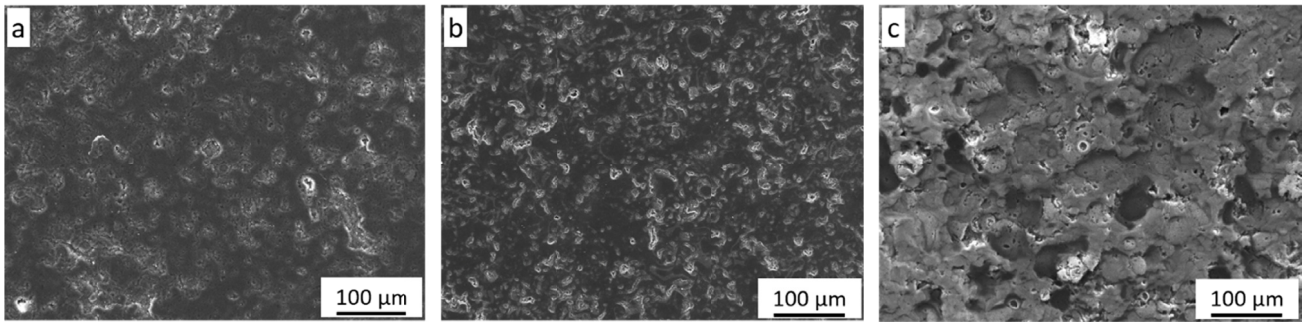

Fig. 3. Surfaces of coatings after polishing a) Al_2O_3-3TiO_2 C; b) Al_2O_3-13TiO_2 C; c) Al_2O_3-13TiO_2 N

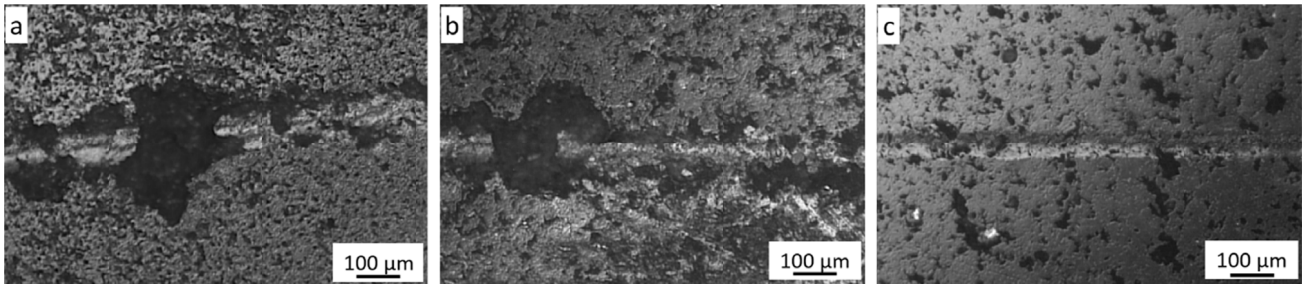

Fig. 4. Microstructure (optical microscope) of wear tracks after scratch test of coatings a) Al_2O_3-3TiO_2 C; b) Al_2O_3-13TiO_2 C; c) Al_2O_3-13TiO_2 N

TABLE 4

Scratch test results for the Al_2O_3-TiO_2 coatings

Coating	$L_{c1\text{-}1}$ [N]	h_{c1} [mm]	$L_{c1\text{-}2}$ [N]	h_{c1} [mm]	FC
Al_2O_3-3TiO_2 C	12 ± 0.5	12 ± 0.5	23 ± 1.6	20 ± 2.6	0.21 ± 0.02
Al_2O_3-13TiO_2 C	16 ± 1.4	15 ± 0.5	23 ± 1.7	20 ± 2.6	0.21 ± 0.02
Al_2O_3-13TiO_2 N	8 ± 0.9	7 ± 0,5	22 ± 2.6	16 ± 1.7	0.16 ± 0.01

Ball on disk tests

Fig. 5 presents the coating friction coefficient curves versus a sliding distance. The friction patterns in samples were produced by abrasive wear due to a sliding contact with the steel ball. It can be seen that the coefficient of friction – sliding distance curves of Al_2O_3-3TiO_2 C and Al_2O_3-13TiO_2 C coatings coupled with steel counterpart shared similar trends. It was shown that, after a short running-in period, about 750 m, the friction coefficients kept at a relative steady-state stage. The nanostructured coating showed a slightly different character of the curve, where after the transient running-in period it maintained an upward trend by keeping a stable value after ~1900 m of the test. However, as can be seen in Fig. 5, the Al_2O_3-13TiO_2 N exhibited a significant reduction of the friction coefficient (0.52 ± 0.02) when compared with that of the conventional coatings under identical wear test conditions. Additionally, the coefficient of friction was found to be a slightly lower for Al_2O_3-3TiO_2 C deposit (0.58 ± 0.04) than that of the Al_2O_3-13TiO_2 C coating (0.62 ± 0.04) after 2000 m

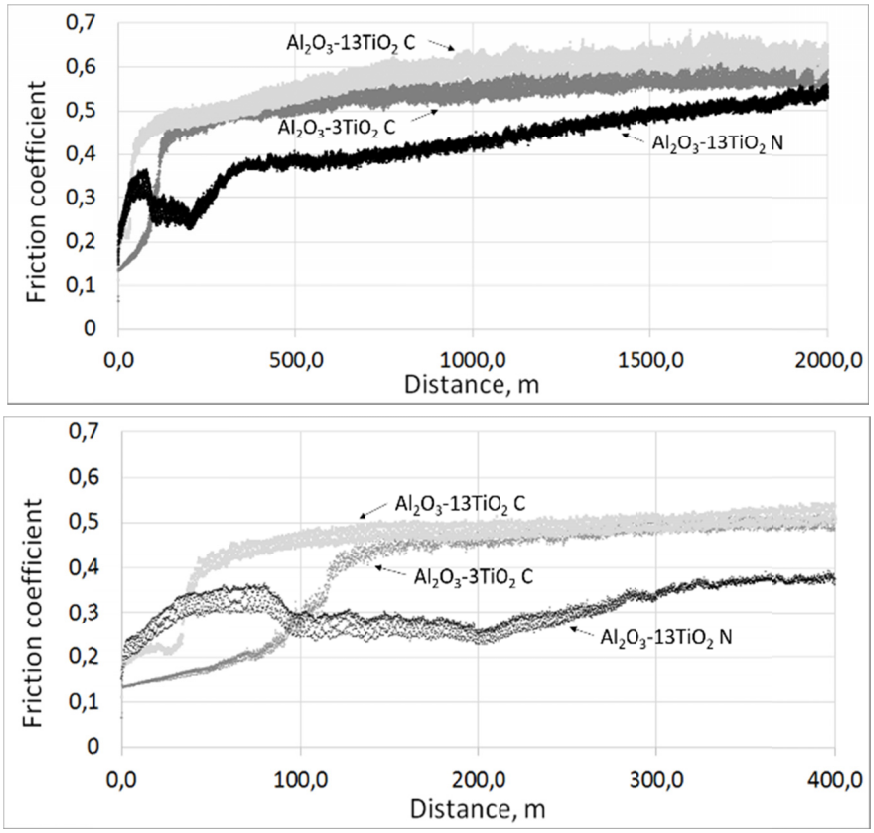

Fig. 5. Variation of the friction coefficient of coatings sliding against 100Cr6 ball

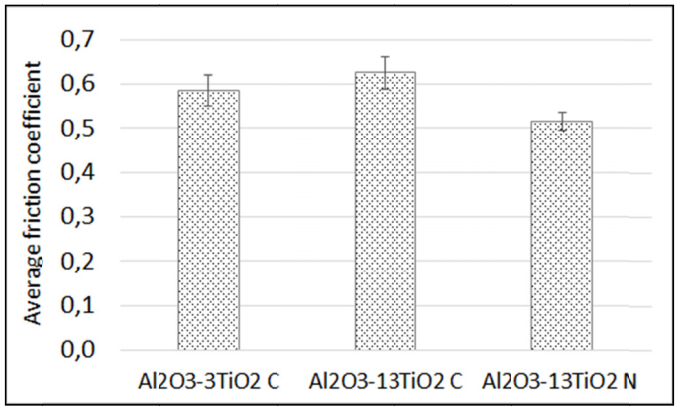

Fig. 6. The average coefficient of friction coupled with 100Cr6 steel counterpart at the end of the test (2000 m)

of a sliding distance, Fig. 6. These obtained results agreed with Fang et al. [36] reporting that the stable friction coefficient was the result of the reduction of wear debris participating in the friction process.

Fig. 7 shows morphologies of the worn surface of the AlO_2-TiO_2 coatings. There were obvious differences in the wear track of the coatings sprayed with the conventional and with nanostructured powders. The wear tracks of the conventional coatings were rougher. There were some grooves especially visible in the case of Al_2O_3-13TiO_2 C coating, Fig. 7b and e. The Al_2O_3-13TiO_2 N coating sprayed with nanostructured powders was smooth without obvious grooves and deformation, Fig. 7c and f. Plastic deformations of coating surface during the tribological test were not observed. The coatings revealed an abrasive wear

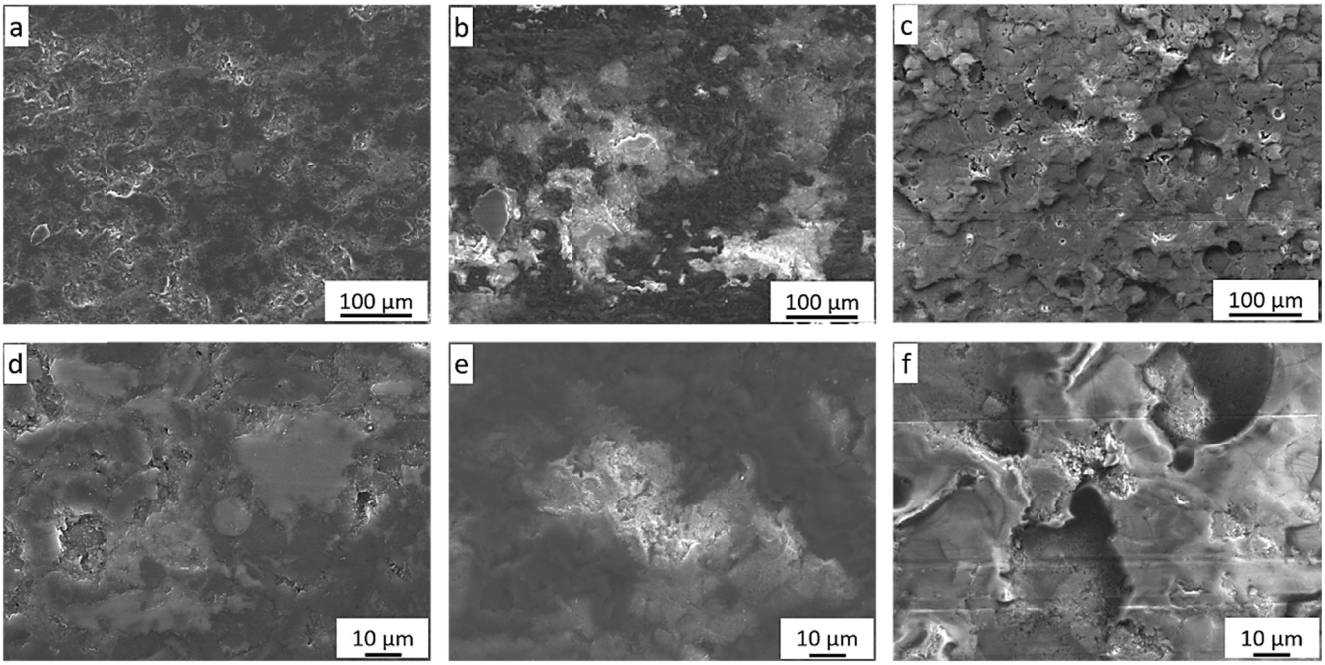

Fig. 7. SEM BSE microstructures at low and high magnifications of wear tracks of coatings in contact with the steel ball 100Cr6 a, d) Al_2O_3-3TiO_2 C; b, e) Al_2O_3-13TiO_2 C and c, f) Al_2O_3-13TiO_2 N

of surface. There were no cracks but there were scratches parallel to the direction of the ball movement, especially visible on the surface of the nanostructured coating. Additionally, in the wear track of Al_2O_3-13TiO_2 C specimen, some ball material was found, which was also confirmed by the profiles in Fig. 8b. By contrast with those deposits, the Al_2O_3-13TiO_2 N coating revealed only a slight wear and represented the smoothest surface, Fig. 7c and f.

The depth of the groove and width of a cross-sectional area of the groove for the coating-steel tribopairs are shown in Fig. 8. There are differences in depth of groove level for the coatings. The highest fluctuating of groove depth with the sliding proceeding revealed the Al_2O_3-13TiO_2 C coating, Fig. 8b. The Al_2O_3-13TiO_2 N deposit exhibited the smallest depth, virtually nil up, Fig. 8c.

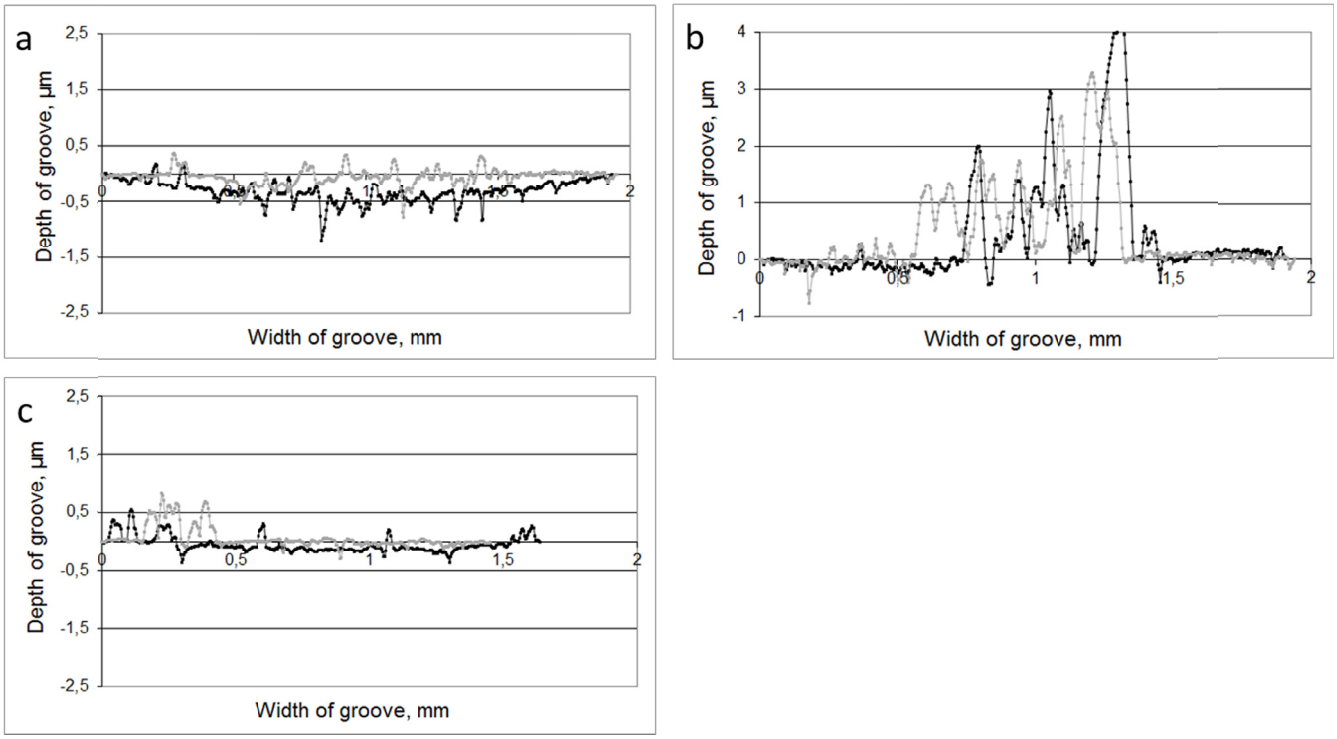

Fig. 8. Selected profiles of the cross-section of wear traces after friction with a ball of 100Cr6 for samples a) Al_2O_3-3TiO_2 C, b) Al_2O_3-13TiO_2 C, c) Al_2O_3-13TiO_2 N

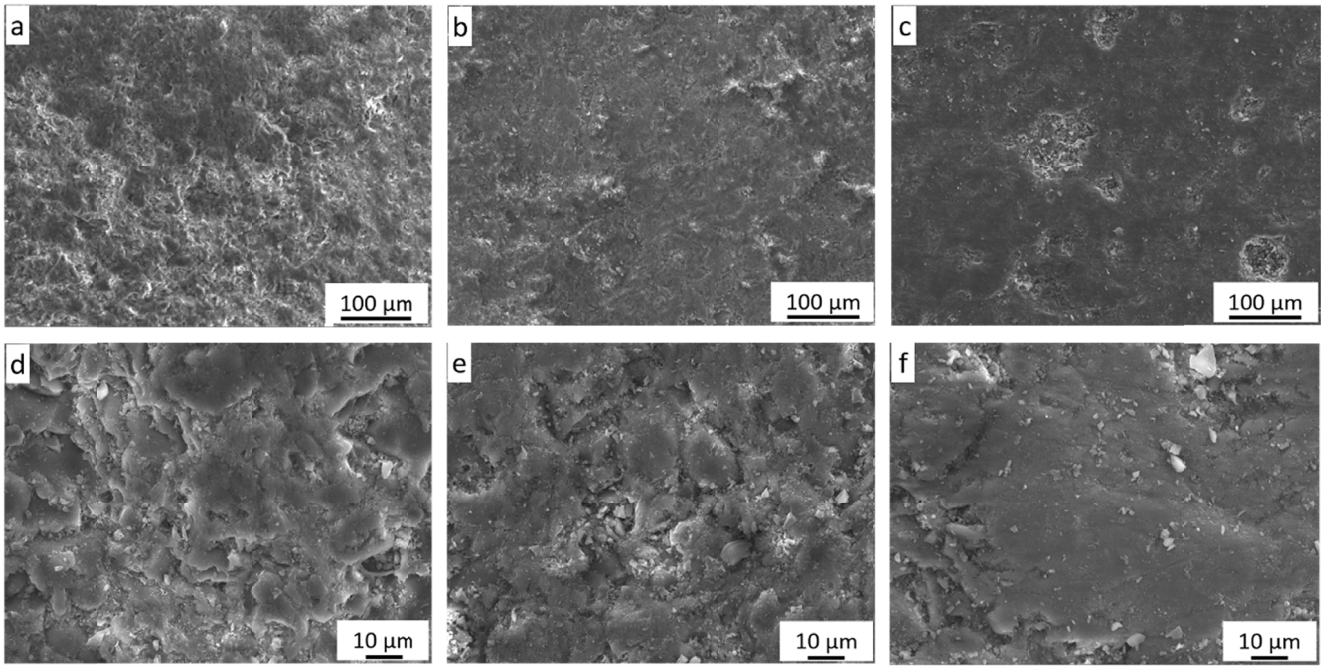

Fig. 9. SEM microstructures after the abrasion test of coatings at low and high magnifications: a, d) Al_2O_3-3TiO_2 C; b, e) Al_2O_3-13TiO_2 C; c, f) Al_2O_3-13TiO_2 N

Friction has been observed in the area of the friction track (Figs. 7 and 8), but the depth of the groove was minimal and not measurable with the available instruments. The measured friction profiles were very different in magnitude and therefore, the wear index determined on its basis was incorrect. Information on the wear resistance of the coatings was obtained indirectly by measuring the wear of the balls, Table 5. The abrasive wear of the balls was observed during the friction of the steel ball with the tested samples. After the wear test, the surface of the balls had distinct scratches and grooves parallel to the direction of movement. The similar diameters of the balls testified their uniform abrasion and lack of worn-out groove in the examined samples. The volume of this wear (V_{ball}) was determined by measuring the diameter of the grinding tip of the ball using an optical microscope. A volumetric wear index of the ball was determined according to the following $W_{s(ball)} = V_{ball}/F_n \cdot s$ [mm^3/N·m] where V_{ball} – the volume of ball material, F_n – normal force, s – friction way.

Results in Table 5 showed that the highest wear was observed in the case of ball sliding on the surface of the nanostructured coating. It evidenced the best tribological properties of this coating. The conventional Al_2O_3-3TiO_2 C coatings revealed the worst wear resistance.

Abrasion resistance

Fig. 9 presents SEM microstructures of the coatings after the abrasion test with 300 µm grain size Al_2O_3 powder used as the abrasive. They showed wide grooves caused by the removal of material from the sample surface under the applied load. The surface changed from smooth to rough. In the case of nanostructured coating, it appeared that abrasion wear was minimal after both 10 min and 20 min of testing and the wear surface was relatively smooth Figs. 9c, f and 10. The amount

TABLE 5

Diameters (A, B), volume (V_{ball}) and friction wear index ($W_{s(ball)} \cdot 10^{-6}$) of steel ball (100Cr6) after wear test with the Al_2O_3-3TiO_2 C, Al_2O_3-13TiO_2 C, and Al_2O_3-13TiO_2 N coatings

Coating	A [mm]	B [mm]	V_{ball} [mm^3]	$W_{s(ball)} \cdot 10^{-6}$ [mm^3/Nm]
Al_2O_3-3TiO_2 C	1.97	1.97	0.25	24.6
Al_2O_3-13TiO_2 C	1.94	1.96	0.23	23.4
Al_2O_3-13TiO_2 N	1.69	1.69	0.13	13.3

of the Al_2O_3-13TiO_2 N removal material was considerably less about three and two times that of Al_2O_3-3TiO_2 C and Al_2O_3-13TiO_2 C, respectively (Fig. 10). When the microhardness and abrasion wear loss of the coatings were compared, the increase in microhardness caused a decrease in wear loss. It may indicate an extended coating lifetime.

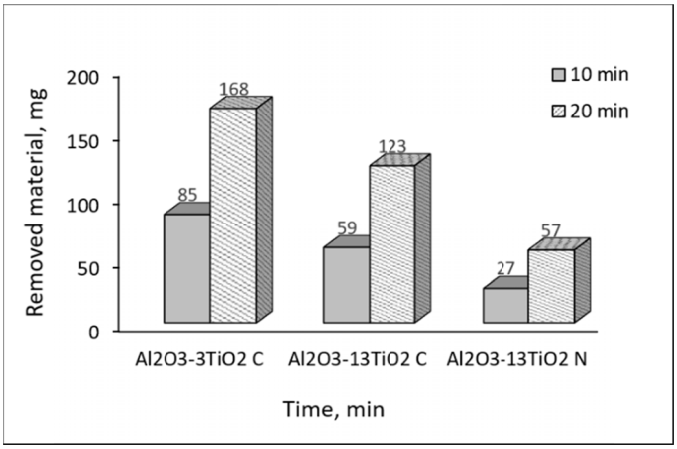

Fig. 10. The removed material of coating surface versus time of abrasive wear of alumina-titania coatings

4. Discussion

Investigations showed that differentiation in the chemical composition and grain size distribution of the feedstock had a significant influence on mechanical and tribological properties of Al_2O_3-TiO_2 plasma sprayed composite coatings. The Al_2O_3-3TiO_2 C coating obtained from the powder containing the smallest volume fraction of TiO_2 revealed the worst properties compared to both conventional and nanostructured Al_2O_3-13TiO_2 coatings. Although the Al_2O_3-13TiO_2 C powder had about twice the grain size of Al_2O_3-3TiO_2 C, it formed the coating of ~30% higher hardness and 20% higher Young's modulus. This coating also showed significantly better wear resistance compared to a coating containing less TiO_2 phase. Regarding tribological properties, both conventional coatings revealed similar values of friction coefficients determined during scratch tests and when they coupled with 100 Cr6 steel counter-part. Any cracks were not observed in the wear tracks of the coatings. However, the Al_2O_3-13TiO_2 C deposit showed a significantly higher resistance (~36 %) to the abrasive wear against Al_2O_3 (300 μm) powder used as the abrasive. Vargas et al. also showed that the wear resistance of Al_2O_3-13TiO_2 coatings was higher than that of Al_2O_3-43TiO_2 [25].

The Al_2O_3-13TiO_2 C coating revealed better abrasive wear resistance and microhardness than the Al_2O_3-3TiO_2 C coating. Sert et al. [37] also showed that the conventional coating with high microhardness had improved wear resistance. In addition, Palacio et al. [38] reported that Al_2O_3-TiO_2 coatings having higher hardness exhibited higher drilling resistance (lower drill depth). In turn, Habib et al. [24] showed the abrasive wear resistance of alumina-titania coatings was inversely proportional to their hardness. The lower microhardness of the coating could be a result of its greater porosity and the presence of softer γ-Al_2O_3 phase as well as TiO_2. Although, the Al_2O_3-13TiO_2 C coating contained more titania phase than Al_2O_3-3TiO_2 C coating it revealed the better mechanical properties and significant abrasion resistance improvement. It could be due to the fact, that the entire α-Al_2O_3 phase did not transform into γ-Al_2O_3 during spraying of Al_2O_3-13TiO_2 C, and therefore, more α-Al_2O_3 phase retained in the microstructure. Additionally, the presence of TiO_2 significantly reduces the melting temperature of the feedstock producing less porous deposits [24,26,39]. The melting temperature decreased because it is significantly lower for TiO_2 (1854°C) than Al_2O_3 (2040°C) and due to titania ability to form a liquid solution with Al_2O_3 [35,37].

As the research showed, the size of the used powder grain more than the titania content influenced the properties of the deposited coatings. The nanostructured coating revealed the best mechanical and tribological properties. The microhardness, Young's modulus, fracture toughness and friction coefficient were up to 25% better than that of the conventional coatings with the same volume fraction of TiO_2 phase. The wear (ball on disk) tests showed that the coatings deposited with the nanostructured powder were more resistant to wear than both the coatings obtained from the conventional feedstock. The improved wear resistance in the nanostructured coatings was the result of an increase in the fracture toughness and a decrease in frictional force. It is worth emphasizing that these coatings showed more than 50% better abrasion resistance. Similar studies on the abrasive wear showed that nanostructured coatings revealed a considerable increase in the wear resistance in comparison with the conventional coatings [6,19,21-23]. The surface roughness of all coatings was nearly the same, so the microstructure and mechanical properties of these deposits were important factors which influenced the abrasive wear resistance. In the case of nanostructured coatings, their mechanical and tribological properties improvement was mainly related to the bi-modal microstructure formed by fully and partially melted initial particles and grain refinement. The partially melted α-Al_2O_3 particles were a retained part of the initial nanostructure surrounded by a three-dimensional net-like structure formed from fully melted oxides (Al_2O_3, TiO_2, ZrO_2, CeO_2). The presence of α-Al_2O_3 particles along with rapidly solidified γ-Al_2O_3 into which Ti, Zr and Ce elements were dissolved and being existed in nanocrystalline sizes produced the composite coating with improved mechanical and tribological properties. Moreover, the α-Al_2O_3 as an elastically stiffer phase offered resistance to cracks propagating and toughening mechanisms, such as crack bridging and crack deflection [40]. Jordan et al. and Gell et al. [15-16] reported that the nanostructured Al_2O_3-TiO_2 coatings had excellent resistance to crack propagation after the bend and cup test as well as scratch test. Moreover, they explained the improved resistance by the arrest and deflection of the crack propagation in partially melted regions. The presented results indicated the potential of nanostructured coatings that provide a substantial improvement in wear resistance compared to the conventional coatings.

5. Conclusions

The paper presents how different volume fraction (3 wt.% and 13 wt.%) of TiO_2 phase in the Al_2O_3-TiO_2 conventional feedstock and the grain size distribution (conventional and nanostructured) of the powder influenced the mechanical and tribological properties of plasma sprayed coatings on steel substrates. The significance of the presented studies are pointed below:

1. The grain size of the feedstock powder had stronger than the titania phase content influence on the properties of plasma sprayed coatings. The nanostructured Al_2O_3-13TiO_2 coatings revealed the best mechanical and tribological properties.
2. Microhardness of the coatings affected their wear-resistance property. The nanostructured coatings with the highest hardness had the best wear resistance. The improved wear resistance was the result of the bi-modal microstructure of the coating created by partially melted particles of initial powders embedded in the nanocrystalline matrix formed from fully melted oxide particles.
3. The nanostructured coatings demonstrated a 50 % increase in the abrasion wear resistance compared to the conventional coatings.

4. The increase in TiO_2 content from 3 wt.% to 13 wt.% of the feedstock improved the mechanical properties and abrasion resistance of the conventional coatings.

REFERENCES

[1] H. Yamakiri, S. Sasaki, T. Kurita, N. Kasashima, Tribol. Int. **44**, 579-584 (2011).

[2] G. Di Girolamo, A. Brentari, C. Blasi, E. Serra, Ceram. Int. **40**, 12861-12867 (2014).

[3] V. Fervel, B. Normand, C. Coddet, Wear **230**, [1] 70-77 (1999).

[4] H. Luo, P. Song, A. Khan, J. Feng, J.J. Zang, X.P. Xiong, J.G. Lü, J.S. Lu, Ceram. Int. **43**, 7295-7304 (2017).

[5] N. Dejang, A. Watcharapasorn, S. Wirojupatump, P. Niranatlumpong, S. Jiansirisomboon, Surf. Coat. Technol. **204**, 1651-1657 (2010).

[6] R. Yilmaz, A. O. Kurt, A. Demir, Z. Tatli, J. Eur. Ceram. Soc. **27**, 1319-1323 (2007).

[7] L.L. Shaw, D. Goberman, R. Ren, M. Gell, S. Jing, Y. Wang, T.D. Xiao, P. R. Strutt, Surf. Coat. Technol. **130**, 1-8 (2000).

[8] D. Goberman, Y. Sohn, L. Shaw, Acta. Mater. **50**, 1141-1152 (2002).

[9] X. Lin, Y. Zeng, C. Ding, P. Zhang, Wear **256**, 1018-1025 (2004).

[10] A.A. Kulkarni, S. Sampath, H. A. Goland, H. Herman, B. Dowd, Scr. Mater. **43**, 471-476 (2000).

[11] P. Bansal, N. Padture, A. Vasiliev, Acta. Mater. **51**, 2959-2970 (2003).

[12] W.Tian, Y. Wang, Y. Yang, C. Li, Surf. Coat. Technol. **204**, 642-649 (2009).

[13] A. Rico, C.J. Múnez, J. Rodríguez, Surf. Coat. Technol. **243**, 46-50 (2014).

[14] F.J. Gammel, D.P. Jonke, O. Rohr, "Nanopowders – an approach to enhanced surface coatings" pp. 261-272 in Nanostructured thin films and nanodispersion strengthened coatings, ed. by A.A. Voevodin, Netherlands: Kluwer Academic Publisher 2004.

[15] E.H. Jordan, M. Gell, Y.H. Sohn, D. Geberman, L. Shaw, S. Jiang, M. Wang, T.D. Xiao, Y. Wang, P. Strutt, Mater. Sci. Eng. A **301**, 80-89 (2001).

[16] M. Gell, E.H. Jordan, Y.H. Sohn, D. Goberman, L. Shaw, T.D. Xiao, Surf. Coat. Technol. **146-147**, 48-54 (2001).

[17] H. Luo, D. Goberman, L. Shaw, M. Gell, Mater. Sci. Eng. A **346**, 237-245 (2003).

[18] L. Pawlowski, Surf. Coat. Technol. **202**, 4318-4328 (2008).

[19] M. Wang, L. L. Shaw, Surf. Coat. Technol. **202**, 34-44 (2007).

[20] Y. Yang, Y. Wang, W. Tian, D. Yan, J. Zhang, L. Wang, Mater. Des. **65**, 814-822 (2015).

[21] X. Lin, Y. Zeng, C. Ding, P. Zhang, Tribol. Lett. **17**, 19-26 (2004).

[22] J. Ahn, B. Hwang, E.P. Song, S. Lee, N.J. Kim, Metall. Mater. Trans. A **37A**, 1851-1861 (2006).

[23] V.P. Singh, A. Sil, R. Jayaganthan, Mater. Des. **32**, 584-591 (2011).

[24] K.A. Habib, J.J. Saura, C. Ferrer, M.S. Damra, E. Giménez, L. Cabedo, Surf. Coat. Technol. **201**, 1436-1443 (2006).

[25] F. Vargas, H. Ageorges, P. Fournier, P. Fauchais, M.E. López, Surf. Coat. Technol. **205**, 1132-1136 (2010).

[26] E. Klyatskina, E. Rayón, G. Darut, M.D. Salvador, E. Sánchez, G. Montavon, Surf. Coat. Technol. **278**, 25-29 (2015).

[27] S. Jia , Yong Zou, J. Xu, J. Wang , L. Yu, Trans. Nonferrous Met. Soc. China, **25**, 175-183 (2015).

[28] X. Lin, Y. Zeng, C. Ding, P. Zhang, Wear **256**, 1018-1025 (2004).

[29] S. Guessasma, M. Bounazef, P. Nardin, T. Sahraoui, Ceram. Int. **32**, 13-19 (2006).

[30] J.J. Kang , B.S. Xu, H.D. Wang, C.B. Wang, Physics Proc. **50**, 169-176 (2013).

[31] W.C. Oliver, G.M. Pharr, J. Mater. Res. **7** (6), 1564-1583 (1992).

[32] W. Żórawski, A. Góral, O. Bokuvka, L. Lityńska-Dobrzyńska, K. Berent, Surf. Coat. Technol. **268**, 190-197 (2015).

[33] Y. Yang, Y. Wang, Z. Wang, G. Liu, W. Tian, Mater. Sci. Eng. A **490**, 457-464 (2008).

[34] S. Sathish,M. Geetha, S.T. Aruna, N. Balaji, K.S. Rajam, R. Asokamani, Wear **271**, 934-941 (2011).

[35] A. Góral, L. Lityńska, W. Żórawski, Mater. Charact. 96, 234-240 (2014).

[36] Y. Fang, Y. Zhang, H. Fan, T. Hu, J. Song, L. Hu, Wear **334-335**, 23-34 (2015).

[37] Y. Sert, N. Toplan, Adv. Mat. Res. **47**, 181-183 (2013).

[38] C.C. Palacio, H. Ageorges, F. Vargas, A.F. Díaz, Surf. Coat. Technol. **220**, 144-148 (2013).

[39] S.H. Yao, Y.L. Su, W.X. Kao, Adv. Mater. **328**, 853-856 (2011).

[40] J. Rodriguez, A. Rico, E. Otero, W.M. Rainforth, Acta Mater. **57**, 3148-3156 (2009).